Suyehiro, K., Sacks, I.S., Acton, G.D., and Oda, M. (Eds.)
Proceedings of the Ocean Drilling Program, Scientific Results Volume 186

17. Data Report: Triaxial Shear Strength Investigations of Sediments and Sedimentary Rocks from the Japan Trench, ODP Leg 186[1]

S. Roller,[2] C. Pohl,[2] and J.H. Behrmann[2]

ABSTRACT

In order to determine the shear parameters of the forearc sedimentary strata drilled during Ocean Drilling Program Leg 186, West Pacific Seismic Network, Japan Trench, eight whole-round samples were selected from different depths in the drilled sections of Sites 1150 and 1151. Whereas Site 1150 lays above the seismically active part of the subduction zone, Site 1151 is situated in an aseismic zone. The aim of the triaxial tests was, apart from determination of the static stress strain behavior of the sediments, to test the hypothesis that the static stress strain parameter could differ for each sites. In order to simulate undrained deformation conditions according to the high clay mineral content of the strata, consolidated undrained shear tests were performed in a triaxial testing setup. Measurements of water content, grain density, organic content, and microtextural investigations under the scanning electron microscope (SEM) accompanied the compression experiments. After the saturation and consolidation stages were completed, failure occurred in the compression stage of the experiments at peak strengths of 280–7278 kPa. The stiffness moduli calculated for each sample from differential stress vs. strain curves show a linear relationship with depth and range between 181 and 5827 kPa. Under the SEM, the artificial fault planes of the tested specimen only show partial alignment of clay minerals because of the high content of microfossils.

[1]Roller, S., Pohl, C., and Behrmann, J.H., 2003. Data report: Triaxial shear strength investigations of sediments and sedimentary rocks from the Japan Trench, ODP Leg 186. *In* Suyehiro, K., Sacks, I.S., Acton, G.D., and Oda, M. (Eds.), *Proc. ODP, Sci. Results,* 186, 1–19 [Online]. Available from World Wide Web: <http://www-odp.tamu.edu/publications/186_SR/VOLUME/CHAPTERS/115.PDF>. [Cited YYYY-MM-DD]
[2]Geologisches Institut der Universität Freiburg, Albertstrasse 23b, D-79104 Freiburg, Germany. Correspondence author: **sybille.roller@uni-bonn.de**

Initial receipt: 7 January 2002
Acceptance: 6 March 2003
Web publication: 30 June 2003
Ms 186SR-115

INTRODUCTION

The data presented stem from a suite of geotechnical experiments carried out on whole-round samples drilled during Ocean Drilling Program (ODP) Leg 186, West Pacific Seismic Network, Japan Trench. The scientific objectives of the cruise were the installation of two in situ measurement devices (seismometers, strainmeter, and tiltmeter) (for details see the Leg 186 *Initial Reports* volume [Sacks, Suyehiro, Acton, et al., 2000]) in the forearc of the Japan Trench at Sites 1150 and 1151. The measurements may help explain why there are seismic (Site 1150) and aseismic (Site 1151) domains in the forearc. Laboratory triaxial deformation tests on eight samples from different depths in the two drilled sections (see Table **T1**) should provide information on the static stress strain behavior of the sedimentary rocks of both sites.

T1. Samples, testing program, and test results, p. 15.

Triaxial tests are a useful tool to determine deformation-specific properties of rocks under realistic conditions (i.e., a cylindrical specimen is subjected to a confining pressure comparable to the horizontal stress in the Earth's crust). Vertical stress resulting from lithostatic overload is simulated by axial piston loading. The vertical load is increased until failure occurs. From the possible types of triaxial tests, the consolidated undrained (CU) test is considered to be most suitable to simulate abrupt earthquake-induced deformation, a buildup of pore pressure, which results from impeded drainage in the clayey sediments and sedimentary rocks. In contrast, the consolidated drained (CD) test permits the escape of pore water without an increase of pore pressure. Deformation rates during CD tests are 10 times lower than those of CU tests.

Some samples were cut in several orientations to the artificially generated fault surface and were prepared for the scanning electron microscopy (SEM) to investigate the characteristics and development of the pore space with depth, as well as, the orientation and microstructures of the platy and clayey mineral components on the artificial fault plane surfaces.

METHODS

Standard triaxial tests are symmetrical compression tests on cylindrical samples, primarily performed to determine the shear strength of a material. The experiments were carried out using an ELE Tritest 50 setup, with a maximum cell pressure of 1700 kPa and maximum vertical load of 7500 N (Fig. **F1**). The horizontal stresses ($\sigma_2 = \sigma_3$) are imposed by water pressure; the vertical stress (σ_1) is imposed by piston load and water pressure ($\sigma_1 = F/A + \sigma_3$, with F = piston load and A = area). The water used for external and internal application of pressure to the specimen has to be de-aired to avoid measurement errors due to compressibility of the gaseous phase. The cylindrical triaxial cell encloses the specimen, which is installed on the cell base. The cell base contains the influx to and drainage off the cell and the specimen (Fig. **F1**). The outlets and inlets are each equipped with electrical sensors and connected through piping with either hydraulic pumps (water supply) or with measuring devices (volume change unit and pressure gauges).

F1. Triaxial test setup, p. 9.

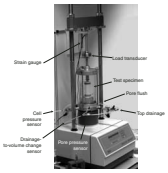

The tests were carried out according to the instructions and recommendations for the determination of shear strength given by the German Institute for Standardization (DIN 18 137, 1990; see parts 1 and 2) and are characterized by three stages: (1) saturation, (2) consolidation,

and (3) compression. Saturation pore pressure is a kind of passive pore pressure induced in the specimen by a hydraulic pump. The pore pressure during consolidation and compression stages is defined as back pressure, as it rises in the tested specimen as a reaction to cell pressure and piston load.

Basically, a series of three tests at different confining pressures must be conducted to construct the Mohr-Coulomb envelope in the shear stress (τ) vs. normal stress (σ_n) diagram. Limited sample volume, due to fracturing and required sample size, restricted the number of tests per whole-round sample to only two at different cell pressures, or even only one. This circumstance reduces the accuracy of Mohr-Coulomb envelopes and makes determinations of shear parameters less precise.

As mentioned before, failure of the sample is induced by a piston advancing at constant speed (for velocities for each sample see Table **T1**), causing increasing vertical stress (σ_1). The development of the vertical force is measured by a load transducer. The tests are run until an ultimate condition is reached (Head, 1986). Failure criteria can serve both the peak differential stress, where shear strength of the sample is exceeded, or a limiting strain of 15%–20% for plastically deforming soils. The axial shortening is measured by a strain-gauge sensor (Fig. **F1**). During undrained tests, the drainage system is locked and a pore pressure builds up as a result of compression. The vertical load and the displacement of the piston are measured by the load transducer and strain gauge sensor in time intervals, depending on the amount of change of these quantities. Except for the deepest sample from Site 1151, the strength of which exceeded the limit force of the load transducer unit, all tests were carried out until the failure criteria were reached. Two samples from Section 186-1151A-84R-2 were analyzed using drained shear tests because of temporarily defective testing conditions. On the one hand, the stiffness moduli obtained are comparable to those of the undrained tests, but on the other hand, we could not infer the cohesion and the internal angle of friction.

According to the size of the cell's base, the samples had diameters of 35 mm. However, as most of the cores from Site 1150 underwent postdrilling stress relaxation (Figs. **F2, F3**), in most cases, only cylinders with diameters of 24 mm could be carved out. Sample preparation included sawing of the whole-round cores into pieces of required length, which amounted to 2–2.5 times the diameter. With the aid of a hand-operated soil lathe, the samples were cut and rasped into a cylindrical shape with a constant diameter of 35 mm (Head, 1982). Specimens with diameters <35 mm had to be prepared without the lathe. The top and bottom surfaces of the cylinders had to be cut off evenly and parallel to each other to avoid strain concentrations at the piston/specimen interface (Jaeger and Cook, 1979). The sample preparation had to be done very carefully to avoid disturbance of texture and cohesion. Before being installed into the cell, the specimen was wrapped in filter-paper side drains. Afterward, porous disks were fitted to both ends of the filter-wrapped cylinder before it was inserted into an impermeable rubber membrane. This drainage assemblage allowed an optimum of water flux in a vertical as well as horizontal direction and a homogeneous distribution of pore water pressure. With the setup and sample preparation described, a natural-rock surrounding could be roughly modeled. Parallel to the preparation of the cylinders, the water content and grain density were determined (Table **T1**). Porosity data were simply adopted from the shipboard measurements (Sacks, Suyehiro, Acton, et al., 2000).

F2. Postdrilling stress relaxation fracture, p. 10.

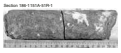

F3. Relaxation phenomena, p. 11.

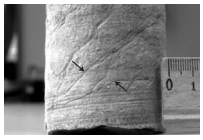

After the sample was installed in the cell and connected to the top and base drainage system (Fig. F1), the cell and the connecting pipes were flooded with de-aired water. The general procedure of a CU test is as follows:

1. A defined and reproducible stress state is established in the specimen by saturation and consolidation.
2. The drainage system is closed.
3. Vertical load is increased by continuously displacing the piston downward.

The aim of saturation is to dissolve remaining air in the pore water. Air in the pores corrupts the results of the compression test. To achieve saturation, the cell pressure and the pore pressure are increased simultaneously. The value of necessary saturation pore pressure depends on the initial saturation (S_0) of the material tested:

$$S_0 = (w\rho_s[1 - n])/(n\rho_w)$$

where

S_0 = initial saturation;
w = water content (percent);
ρ_s = grain density (g/cm³);
n = porosity (percent); and
ρ_w = density of water (g/cm³).

According to DIN 18 137 (1990) part 2, initial saturation S_0 between 0.65 and 0.9 requires a saturation pore pressure between 200 and 900 kPa. In all experiments, cell pressure and saturation pressure (σ_p) were increased incrementally in three steps to avoid damage to the sedimentary fabric. The amount of water squeezed into the specimen was measured by the volume change device. A typical pressure-water influx correlation is given in Figure F4. The progress of saturation was controlled by closing the valve to the volume change device and subsequently raising the cell pressure by up to 10%. When saturation is achieved, the ratio of pore pressure change to the cell pressure change must be >0.95. In the clayey sediments and sedimentary rocks tested, the saturation stage lasted an average of 72 hr.

F4. Saturation data, p. 12.

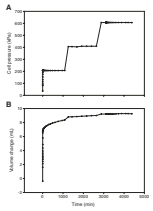

After the completion of saturation, the test specimens were consolidated. The objective of consolidation is to create a defined equilibrium and isotropic stress state before the specimen is loaded to failure. Evidently, the values of consolidation pressure are higher than saturation pressure and are always restricted by the limiting stress value of the measurement device. The pressures were chosen in intervals approximately proportional to the drilling depth of the sections (for applied consolidation pressure values see Table T1). The cell pressure was increased, starting from the final cell pressure of the saturation stage, while the formerly applied saturation pore pressure was maintained. Under these isotropic stress conditions and with open drainage, there was an initial rise in pore pressure followed by a fall due to the dewatering of the specimen into the back pressure system. When the back pressure and volume change reached a constant value with time, the consolidation stage was completed. A typical volume change-time correlation can be seen in Figure F5, which shows a graph with an initially steep slope becoming progressively flatter with time. Consolidation

F5. Consolidation diagram, p. 13.

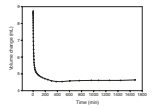

stages usually lasted 25–30 hr. This curve is essential for the calculation of the piston velocity of the compression stage. With the aid of the consolidation, the empirical equation (DIN 18 137, 1990, part 2; Head, 1986) gives the maximum piston velocity for drained tests:

$$\max v = (h \times \varepsilon_f)/(15 \times t_{100})$$

where

max v = maximum rate of deformation (mm/min);
h = height of sample (mm);
ε_f = estimated strain at failure; and
t_{100} = graphically constructed time at 100% consolidation (min).

The calculated rate is valid for CD tests. For CU tests, however, the rate of deformation should be at least 10 times faster. For our tests, we roughly calculated the rate then compared the latter with the order of magnitude recommended in the DIN standard (DIN 18 137, 1990) (depending on the degree of plasticity of the tested material), and, based on the results, determined a rate (Table **T1**). Additionally, the maximum load capacity of the triaxial testing frame (load transducer limit = 7500 N) had to be considered, so lower rates of deformation were chosen for deeper and, hence, stronger samples. In this context, it is worth mentioning the advantage of the small-diameter specimens.

To investigate if and how far clay minerals are oriented in the vicinity of the artificially induced fracture planes, small cubes of material were extracted from Sample 186-1151A-51R-1, 53–63 cm (546 meters below seafloor), in different orientations from the deformed cylinder. After freeze-drying, mounting on aluminium tables, and cathodic sputtering with carbon to make the surface of the subsamples electroconductive, the subsamples were exposed to the electron beam of the SEM. The organic matter content was determined for each tested section as the weight loss after oxidizing the material at 550°C for 2 hr (following the recommendations of DIN 18 121, 1990).

RESULTS

Different modes of failure were observed; most firm and hard samples failed by shear and some of the softer samples showed plastic broadening (see Plates **P1, P2, P3, P4**). Different modes of brittle failure occurred, as there are near-vertical extension fractures, slightly inclined hybrid-extension shear fractures, and shear fractures. Proof for the realistic conditions of the triaxial tests is the perfect parallelism of healed original fractures and artificial shear planes. The fact that a new shear plane was generated instead of reactivating a preexisting discontinuity (Plate **P3,** fig. 1) has an important implication—the inhomogeneity does not influence later deformation in terms of being a location of mechanical weakness. In conclusion, it follows that apart from the need to find intact parts of the cores for preparation of test specimens, there seems to be no need for the samples to be free of healed fractures.

For the evaluation of the results, the effective stresses (σ') have to be calculated, subtracting the measured pore pressure (Δu) from vertical (σ_1) and horizontal (σ_3) stresses.

P1. Samples after testing in triaxial setup, p. 16.

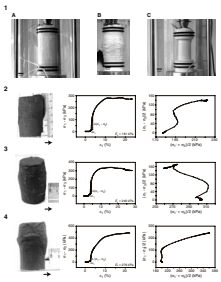

P2. Section 186-1150B-8R-2, p. 17.

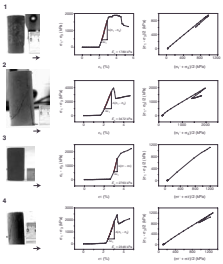

P3. Section 186-1151A-51R-1, p. 18.

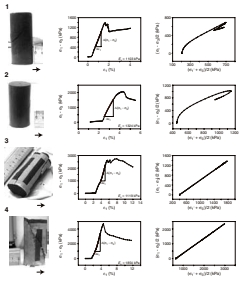

P4. Section 186-1151A-107R-2, p. 19.

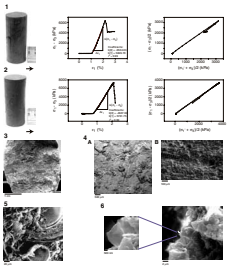

On Plates **P1, P2, P3,** and **P4,** the stress paths ($[\sigma_1'-\sigma_3']/2$ vs. $[\sigma_1'-\sigma_3']/2$) are presented. From the linear (elastic) parts of the $\sigma_1'-\sigma_3'$ vs. ε_1 curves, a stiffness modulus for triaxial compression could be calculated by

$$E_v = \Delta(\sigma_1' - \sigma_3')/\Delta\varepsilon_1$$

with

E_v = stiffness modulus (kPa);
$\Delta(\sigma_1' - \sigma_3')$ = increment of differential stress (kPa); and
$\Delta\varepsilon_1$ = increment of strain (percent).

The stiffness modulus is a measure of the amount of elastic deformation the material can sustain before irreversible plastic or brittle deformation occurs. Figure **F6** shows the stiffness moduli vs. depth at both sites. The stiffness modulus depends on the differential stress evolved during the compression stage. The values increase with depth and, disregarding the Section 186-1151A-107R-2 samples, show an approximately linear rise.

Under the SEM, the slightly polished fault plane of the sample from Section 186-1151A-51R-1 shows a kind of striae or groove-oriented downdip (Plate **P4,** fig. 4a, 4b). An overview of the fracture plane is given in Plate **P4,** fig. 3. The striae can also be observed at this low magnification. Remarkably, at the end of many striae, a fossil impressed into the matrix can be found (Plate **P4,** fig. 4b). Consistently notable is the size of open pore voids, probably leading to a high permeability (Plate **P4,** fig. 5). Observation of the alignment of the clayey minerals was inhibited by the "cemetery" of fossils in the samples. Nevertheless, when we observed clayey minerals on the fault plane, they were present cumulatively (Plate **P4,** fig. 6) or in unique scales on fossil frameworks.

F6. Stiffness modulus vs. depth, p. 14.

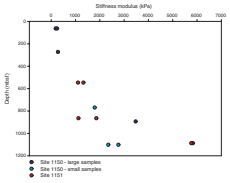

OUTLOOK

Further investigations, such as grain-size analysis and examination of two additional samples under the SEM to be compared to the sample from Section 186-1151-51R-1, will finally complete the data presented here. Results of the construction of the Mohr-Coulomb envelopes and the construction of a "hypothetical" envelope by using the dip angles of the produced failure planes, respectively, will complete the experiments and permit an interpretation of the shear parameters in terms of comparison of both sites.

ACKNOWLEDGMENTS

Many thanks to Volker Feeser for his conscientious review that helped to clarify this data report. We thank Franz Auerbeck who made available the soil lathe. Max Chaplin from ELE considerably helped with a sketch for a proper connection of the setup. Elmar Wosnitza provided physical advice. Matthias Auer examined and corrected the draft and all following versions of the data report. This research used samples and/or data provided by the Ocean Drilling Program (ODP). ODP is sponsored by the U.S. National Science Foundation (NSF) and participating countries under management of Joint Oceanographic Institutions (JOI), Inc. Funding for this research was provided by ODP

Germany. Many thanks to ODP for generously providing the large volume of samples for our tests.

REFERENCES

DIN 18 137, 1990. (German Standard) *Testing Procedures and Apparatus: Triaxial Test, Part 2:* Berlin (Deutsches Institut für Normung).

DIN 18 121, 1976. (German Standard) *Determination of Water Content by Oven Drying*: Berlin (Deutsches Institut für Normung).

Head, K.H., 1982. *Manual of Soil Laboratory Testing* (Vol. 2): *Permeability, Shear Strength and Compressibility Tests:* New York (Halsted Press/Wiley).

————, 1986. *Manual of Soil Laboratory Testing* (Vol. 3): *Effective Stress Tests:* New York (Halsted Press/Wiley).

Jaeger, J.C., and Cook, N.G.W., 1979. *Fundamentals of Rock Mechanics* (3rd ed.): New York (Chapman and Hall).

Sacks, I.S., Suyehiro, K., Acton, G.D., et al., 2000. *Proc. ODP, Init. Repts.,* 186 [CD-ROM]. Available from: Ocean Drilling Program, Texas A&M University, College Station TX 77845-9547, USA.

Figure F1. Triaxial test setup (ELE Tritest 50).

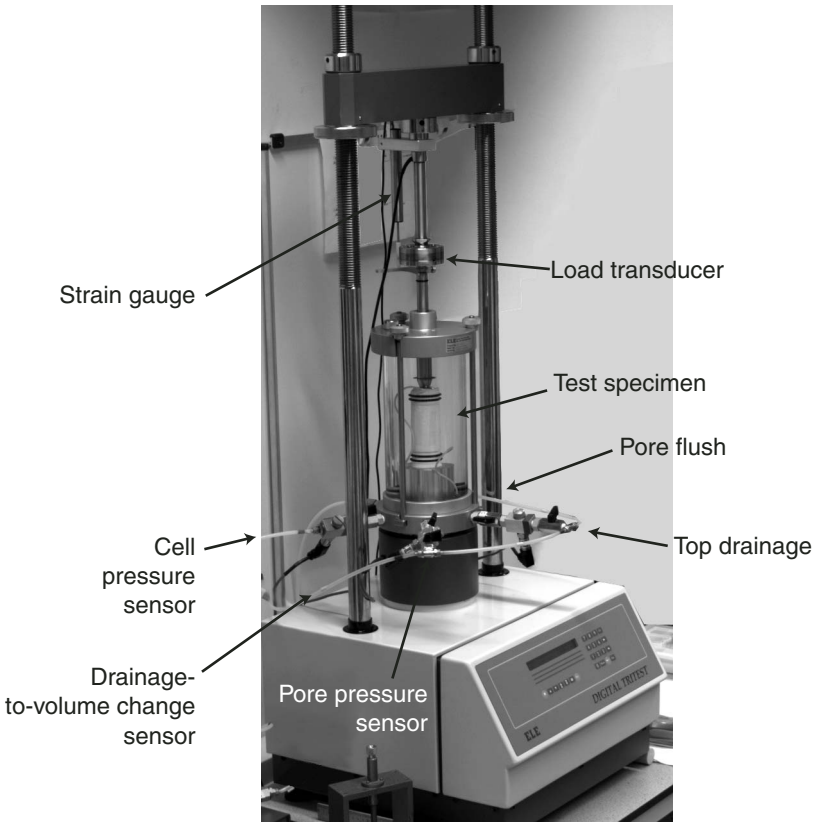

Figure F2. Section 186-1151A-51R-1 shows a large fracture as a result of postdrilling stress relaxation.

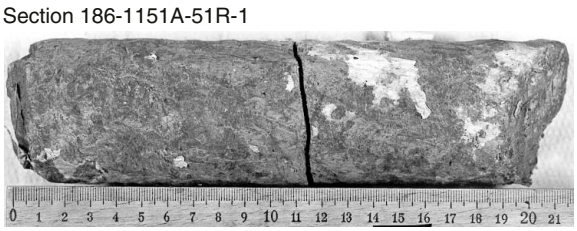

Figure F3. Section 186-1150B-21R-1 relaxation phenomena.

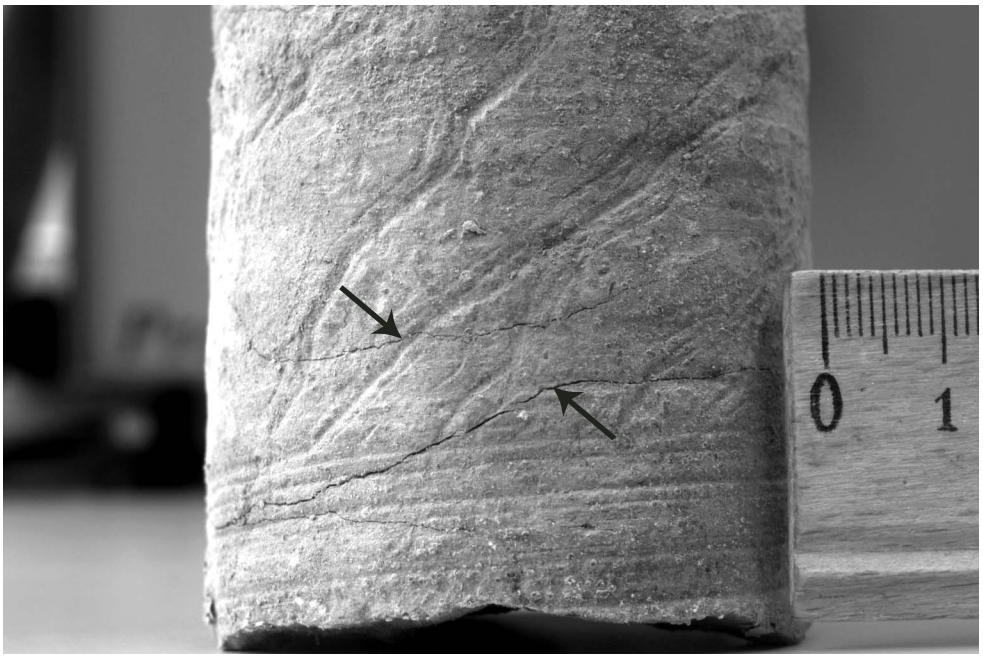

Figure F4. Saturation data (sample 1, Section 186-1151A-51R-1). **A.** Diagram shows the rise of cell pressure in three steps vs. time. **B.** Diagram as a result of parallel rise in cell pressure and pore pressure. The volume change device shows the flux of water into the sample.

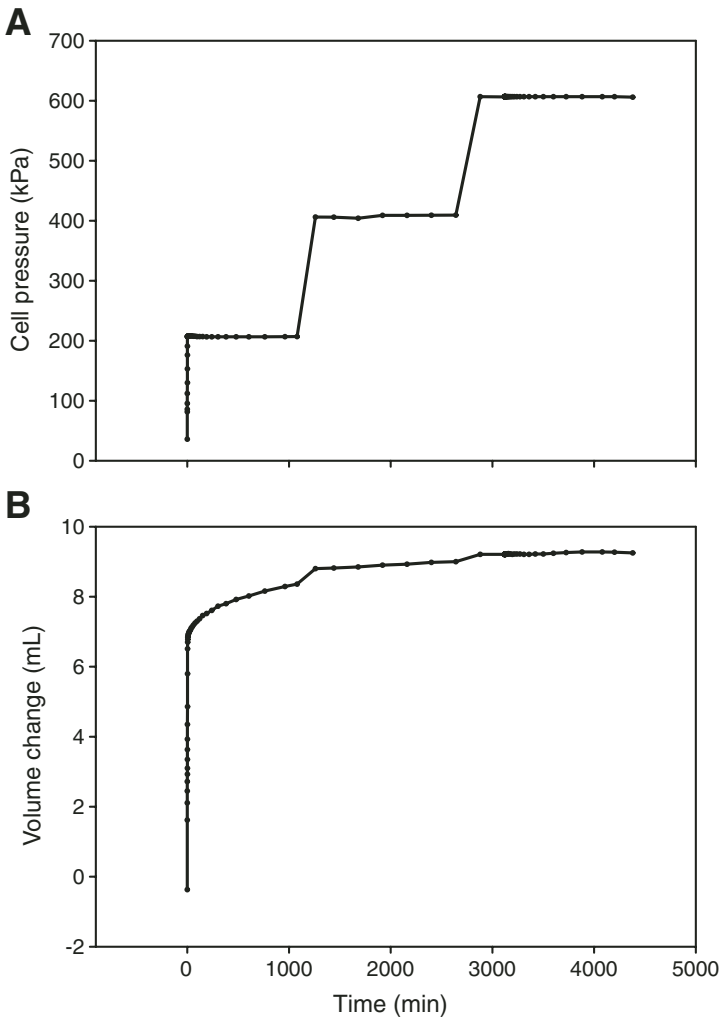

Figure F5. Consolidation diagram (sample 2, Section 186-1150A-7H-6).

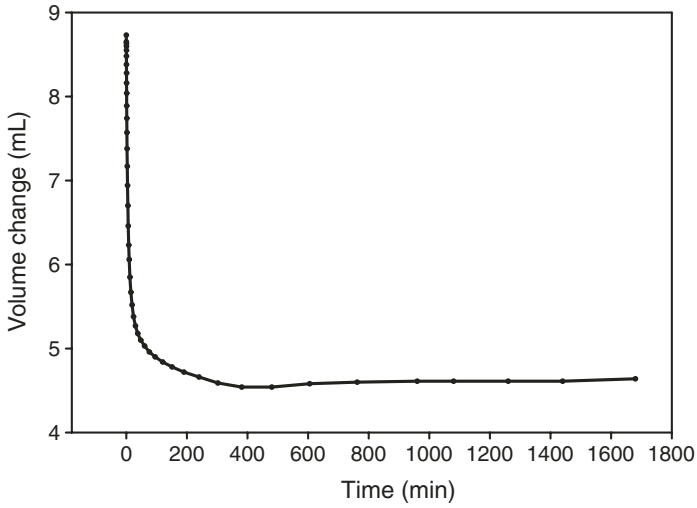

Figure F6. Stiffness modulus vs. depth.

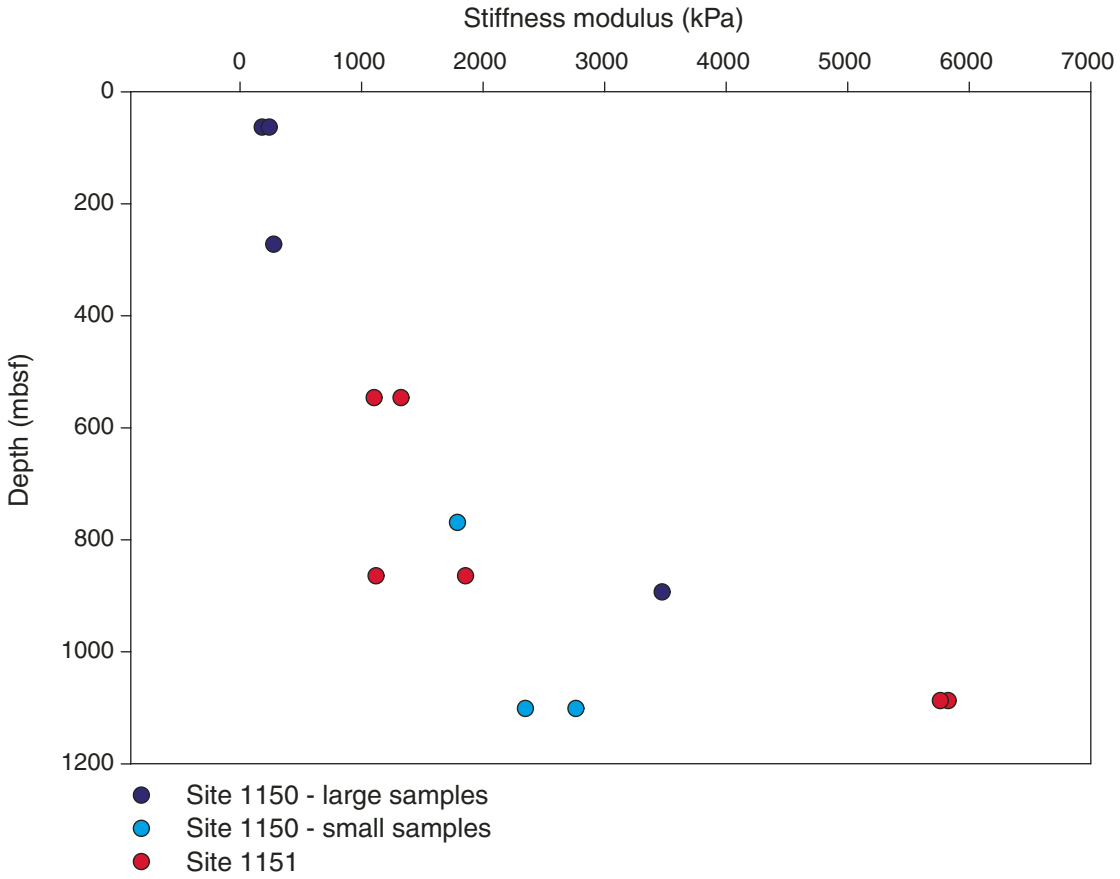

Table T1. List of samples, testing programs, and test results.

Core, section	Depth (mbsf)	Lithology	Induration	Sample number	Test	Height (mm)	Diameter (mm)	Grain density (g/cm^3)	Water content (%)	Organic matter content (%)	Saturation pressure (kPa)	Consolidation pressure (kPa)	Rate of deformation (mm/min)	Yield strength maximum ($\sigma_1 - \sigma_3$) (kPa)	Stiffness modulus E_v (kPa)
186-1150A-															
7H-6	63	Glass diatom spicule-bearing silty clay	Soft	1	CU	73.3	35	2.5	57	4.8	480	630	0.06	280	181
				2	CU	78.5	35		55		530	800	0.06	340	240
30X-2	272	Diatom spicule glass-bearing clay	Soft	1	CU	81	35	2.33	88	5.7	200	400	0.03	485	276
186-1150B-															
8R-2	769	Diatomaceous silty clay	Hard	1	CU	51.8	24	2.18	68	5.9	200	250	0.01	1891	1789
21R-1	893	Diatom glass quartz-bearing silty clay	Hard	1	CU	81.2	35	2.38	37	5.3	750	900	0.008	3912	3472
42R-5	1101	Diatom glass-bearing silty clay	Hard	1	CU	47.5	24	2.27	35	5	250	300	0.008	2211	2763
				2	CU	46.3	24		35		250	355	0.008	2418	2348
186-1151A-															
51R-1	546	Spicule-bearing diatomaceous silty clay	Firm	1	CU	85.2	35	2.18	76	6.5	600	800	0.01	1371	1103
				2	CU	72.5	35		79		600	1050	0.01	2045	1324
84R-2	864	Glass diatom spicule-bearing silty clay	Firm/hard	1	CD	82	35	2.23	49	5.2	900	1300	0.01	5558	1119
				2	CD	82	35		53		900	1545	0.01	4682	1854
107R-2	1087	Glass and spicule-bearing silty clay	Hard	1	CU	85.7	35	2.33	41	4.8	900	1000	0.002	6326	5827
				2	CU	85.9	35		37		900	960	0.002	7278	5762

Note: CU = consolidated undrained, CD = consolidated drained.

Plate P1. Photographs of samples after testing and measurement results of the experiments (graphs showing differential stress vs. strain curves and stress paths). **1.** Samples installed in the triaxial setup. (**A**) Large sample that cultivated a brittle failure (Section 186-1151A-51R-1, sample 2). (**B**) Large sample that shows plastic broadening (Section 186-1150A-7H-6, sample 2). (**C**) Setup for a small sample (Section 186-1150B-8R-2). **2.** Section 186-1150A-7H-6, sample 1. **3.** Section 186-1150A-7H-6, sample 2. **4.** Section 186-1150A-30X-2.

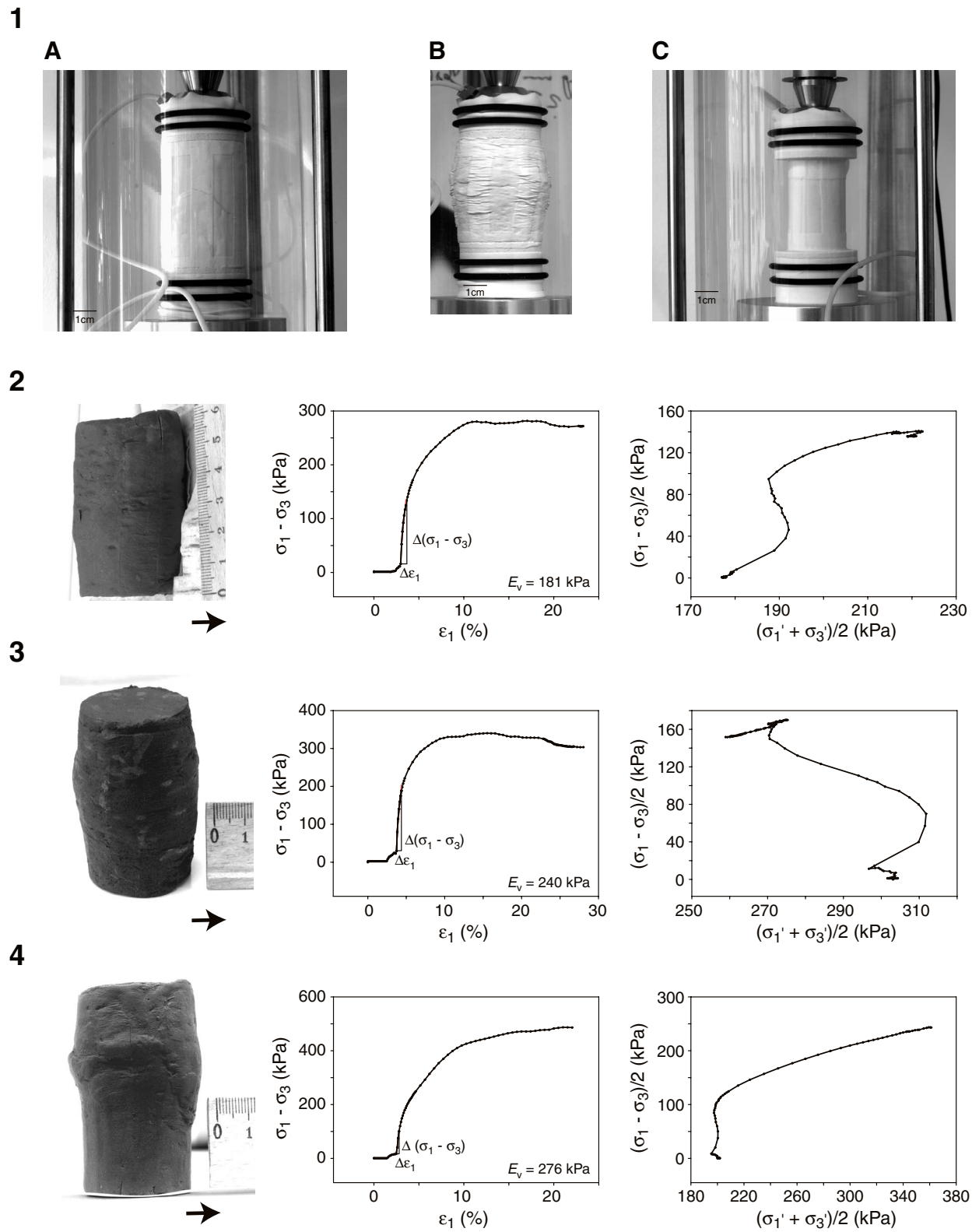

Plate P2. Photographs of samples after testing and measurement results of the experiments (graphs showing differential stress vs. strain curves and stress paths). **1.** Section 186-1150B-8R-2. **2.** Section 186-1150B-21R-1. **3.** Section 186-1150B-42R-5, sample 1. **4.** Section 186-1150B-42R-5, sample 2.

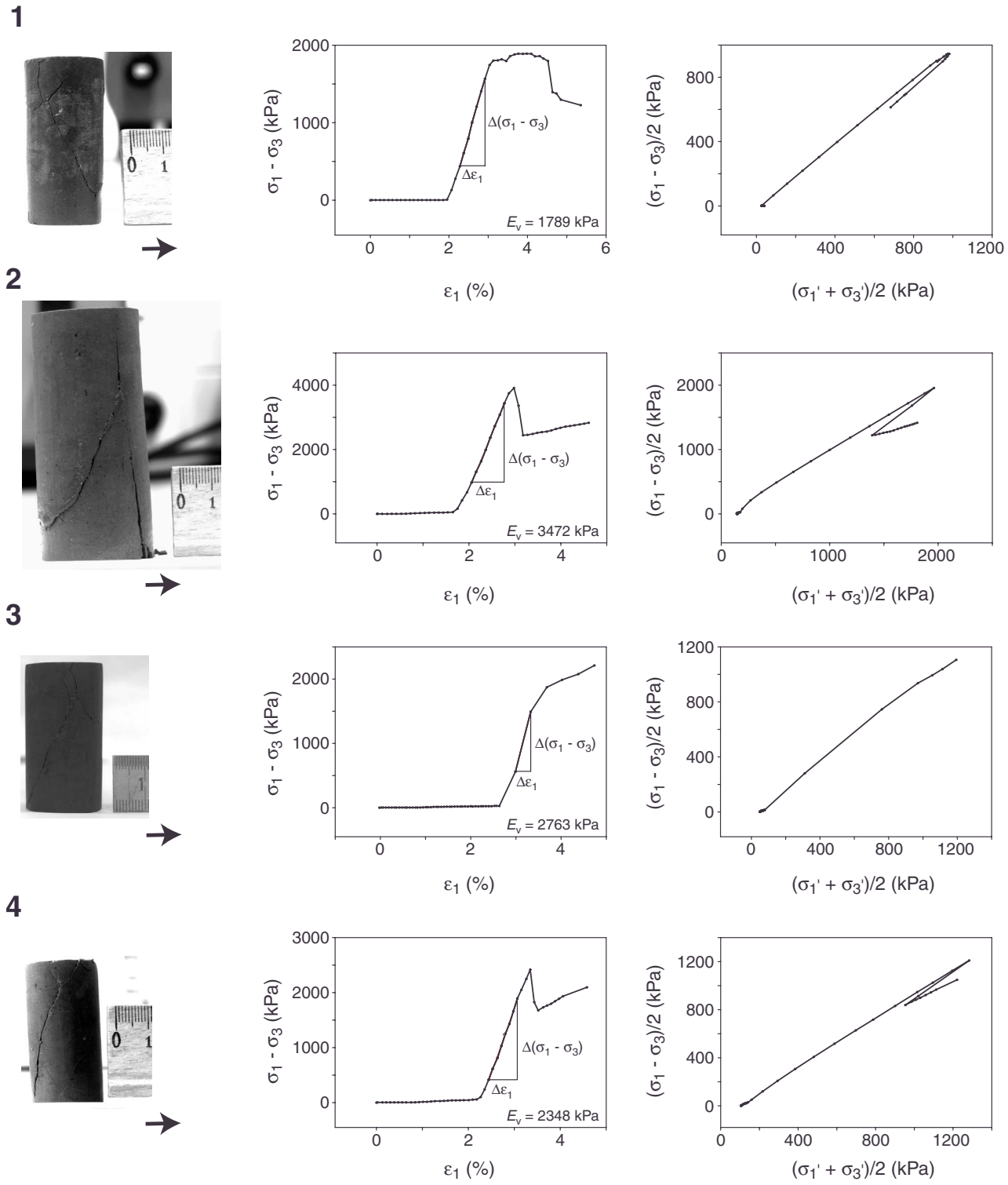

Plate P3. Photographs of samples after testing and measurement results of the experiments (graphs showing differential stress vs. strain curves and stress paths). **1.** Section 186-1151A-51R-1, sample 1. **2.** Section 186-1151A-51R-1, sample 2. **3.** Section 186-1151A-84R-2, drained experiment. Photograph shows sample with filter paper. **4.** Section 186-1151A-84R-2, drained experiment. Photograph shows sample with filter paper.

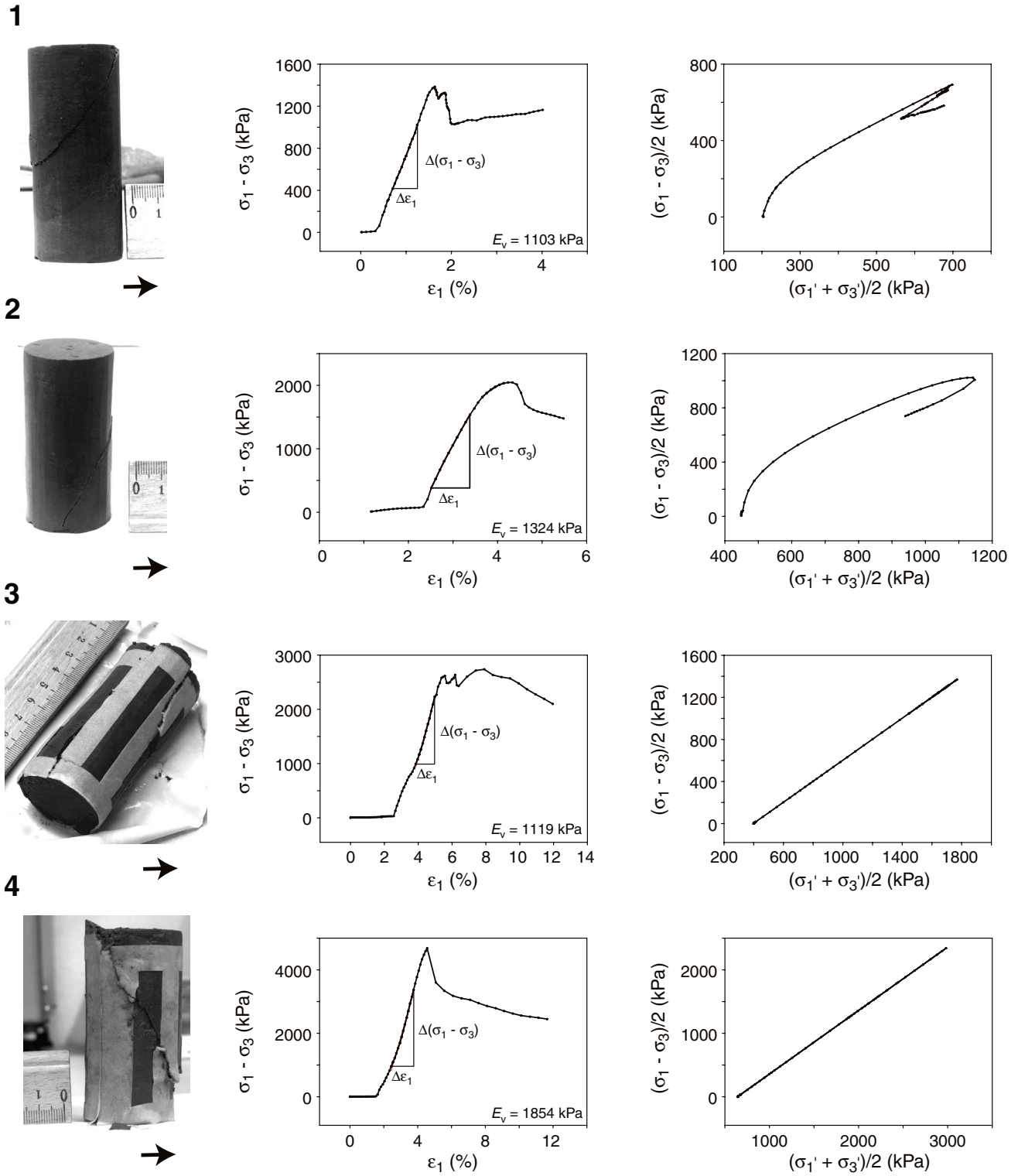

Plate P4. Photographs of samples after testing and measurement results of the experiments (graphs showing differential stress vs. strain curves and stress paths). **1.** Section 186-1151A-107R-2, sample 1. **2.** Section 186-1151A-107R-2, sample 2. **3.** Section 186-1151A-51R-1, sample 1. View of the fracture plane after triaxial test. **4.** Section 186-1151A-51R-1, sample 1, SEM picture. (**A**) Shows striae oriented downdip (BSE mode) with (**B**) detail of (A) showing fossil remains impressed into the matrix at the end of the striae. **5.** Section 186-1151A-51R-1, sample 1, SEM picture. Example of the open pore voids between the fossils. **6.** Section 186-1151A-51R-1, sample 1, SEM picture. Accumulation of clay minerals. Detail shows a single platelet.